International Journal of Networks and Communications 2018, 8(3): 81-96
DOI: 10.5923/j.ijnc.20180803.03

Transmission Performance of Analog Radio-over-Fiber Fronthaul for 5G Mobile Networks

Sara S. Jawad*, Raad S. Fyath

Department of Computer Engineering, Al-Nahrain University, Baghdad, Iraq

Abstract This paper presents the transmission performance of 5G mobile fronthaul based on aggregation of multiple intermediate frequency (IF) over radio-over-fiber platform. Four scenarios describe the environment of single mode fiber (SMF)-link are investigated for efficient bandwidth transmission. The effect of fiber transmission link parameters like dispersion, attenuation, transmission distance, lunch power, and number of aggregated signals are reported for three modulation formats (QPSK, 16QAM, and 64QAM). Increasing the transmission capacity by going towards wavelength division multiplexing is discussed. Simulation results using Optisystem V.14.1 software are presented for 200 MHz- and 1 GHz-bandwidth mobile signals. The simulation reveals that the maximum transmission distance of 16x200 MHz-bandwidth mobile signals over SMF operating with 1550 nm is 82, 69, and 25 km with bit rates 10.24, 20.48 and 30.72 GB/s for QPSK, 16QAM and 64QAM, respectively, at launch power equal 0 dBm. These values are to be compared with 29, 20 and 13 km (9.6, 51.2 and 76.8 Gb/s), respectively, when 8x1 GHz-bandwidth signals are transmitted.

Keywords 5G networks, Radio-over-fiber (RoF), Mobile fronthaul (MFH)

1. Introduction

In recent years, there is rapid evolution of cellular communication technologies toward the 4G Long Term Evolution-Advanced (LTE-A) and higher-generation mobile systems. Low latency and large bandwidth are required to deal with the increasing in data traffic demand to support massive capacity and connectivity. New revolution in wireless system, namely fifth-generation (5G) [1-3], will enhance the data transfer rate of mobile networks, the scalability, the connectivity, and the energy efficiency of the network [4-6]. In 2020, 50 billion devices will be connected to the global IP network [7].

Transport networks will be very important part for the development of 5G networks. It would be constructed using a set of existing technologies, radio-over-fiber (RoF) transmission [8-11] and millimeter wave (MMW) technologies [12-15]. RoF technology incorporates the fiber and the radio wave communication [16]. In conventional wireless communication, mobile fronthaul (MFH) networks are transmission systems which connect central office (CO) and base station (BS) based on wireless communications in microwave (MW) frequency bands. The existing mobile and wireless networks use the MW band of the electromagnetic spectrum for transmission. Thus it is expected that 5G mobile networks can make use of the MMW band efficiently with negligible interference with existing wireless networks [17, 18]. The microwave fronthaul limits the capacity of transmission because of the narrow bandwidths available. Higher data rate can be achieved with operating at MMW bands. The MMW technology opens a new spectral window (30-300 GHz) for next wireless transmission [19, 20]. Further, the high frequencies of MMW carriers enable them to carry higher data rate compared with RF carriers in the MW band [21, 22]. Extensive research has been reported in the literature to use massive multi-input multi-output (MIMO) antenna system [23-25] and orthogonal frequency division multiplexing (OFDM) technique [23], [26-28] for supporting the transmission of 5G services over MMW band. Unfortunately, the atmospheric absorption of the MMW is relatively high which limits the transmission distance below 200 m [19, 29]. The maximum transmission distance depends on the MMW carrier frequency and the atmospheric conditions [20, 30].

To solve the problem associated with high attenuation of MMW transmission, optical fibers can be used as the main transmission link between the main mobile station and the user side [31, 32]. An electrical-to-optical (E/O) and optical-to-electrical (O/E) interfaces are used at both the base station and the user side. The use of RoF technology for transmitting 5G services offers many advantages including security and high bit-rate transmission [26, 33]. The integration of wireless networks with optical networks will

* Corresponding author:
s.jawad12@yahoo.com (Sara S. Jawad)
Published online at http://journal.sapub.org/ijnc

become possible leading to flexible data communication services [34, 35]. Further, RoF technology can support efficiently the use of cloud (or centralized) radio access network (C-RAN) topology which is adopted for 5G wireless networks and can support massive MIMO operation [36, 37]. Beside that, using silicon photonics enables the MMW photonic generation, processing, and transmission of MMW signals which are suitable for RoF systems [38-40].

Mobile fronthaul solution with large data capacity has attract increasing interest especially for 5G mobile networks based on fiber backbone [41-45]. The remote radio units (RRUs) and wireless baseband units (BBUs) are connected via the MFH to support C-RAN. A significant number of distinct BBUs are grouped at a central processing pool [46], as illustrated in Figure 1. Most of previous studies related to RoF-based MFH have used digital optical communication techniques to carry the common public radio interface (CPRI)-formatted signals [47, 48]. Many advantages obtained with CPRI-based MFH such as simplified operations and compensations in long term evolution (LTE) and 4G radio access networks. The in-phase (I) and quadrature (Q) waveforms of the wireless signals are transmitted through the CPRI interface in a binary sequence [49]. The generated binary data will be used to modulate a semiconductor laser using ON-OFF modulation format. The transmitter of the binary digitized CPRI requires high bandwidth especially when large bandwidth aggregated signals are used. For example, 64× 64 massive MIMO with 200 MHz signal bandwidth, for each antenna directional sector the CPRI-equivalent data rate would be about 800 Gb/s. For supporting three directional sectors, the total data rate required by CPRI would be as high as about 2.4 Tb/s [50]. However, transmitting RF signals in digital form for CPRI-formatted frame specifications requires very large transmission bandwidth. To overcome this problem, analog RoF (A-RoF) schemes have been proposed to accommodate more mobile signal channels over a single wavelength leading to higher optical bandwidth efficiency and hence increases the capacity of MFH [51].

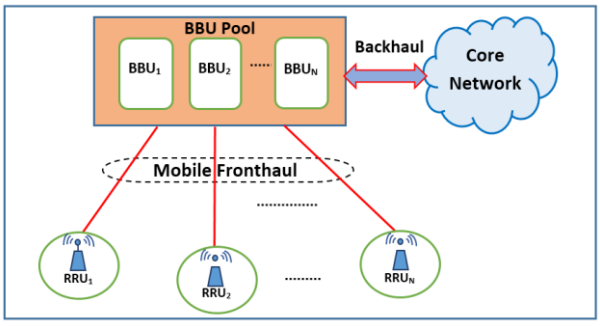

Figure 1. Fronthaul-based C-RAN

Mobile fronthaul schemes based on A-RoF attract increasing interest from cost-effective point of view. Most of these schemes are based on aggregated multiple mobile signals using frequency division multiplexing (FDM) technique [46, 49], [52-54]. The resultant FDM waveform is then converted to analog signal to modulate the optical carrier. Generally, intensity modulator/direct detection (IM/DD) technique is used which is characterized by low-cost implementation compared with coherent detection technique since it does not require a synchronized local oscillator laser at the receiver. The progress in photonic technology enables the implementation of IM/DD optical communication systems operating at bit rate as high as 100 Gb/s [55, 56]. Both direct and external intensity modulation have been investigated in the literature for RoF systems, the latter is more efficient at high bit rate [57-59]. The analog FDM RoF-based MFH has been addressed by different research groups. The concept of this MFH scheme has been applied mainly for aggregated 20 MHz LTE signals [46], [60-61] and 100 MHz LTE-A signals [60] with suggestions for scaling up the fronthaul capacities for future 5G services [46]. Recently, the scheme has been demonstrated experimentally for 5G mobile network in 28 GHz MMW environment supporting 1.5 Gb/s for each user [62].

This paper presents comprehensive investigation for the transmission performance of analog FDM RoF-based MFH for 5G mobile network. Results are presented for the aggregation of multiple 200 MHz- and 1 GHz-bandwidth mobile signals. Both single-optical channel operating at 1550 or 1310 nm carrier wavelength and wavelength division multiplexing (WDM) channels are considered. The simulation results are obtained using the commercial software Optisystem V.14.1.

The aim of the work is to investigate the transmissions performance of 5G services over fiber communication system by investigating the efficient bandwidth of transmission using A-RoF technology. Investigating the effects of fiber transmission link like, dispersion, attenuation, launch power, transmission distance, number of aggregated channels, channel bandwidth, and type of modulation. Also, enhancing the transmission capacity by increasing the number of aggregated channels and going towards WDM system is addressed. The metric used to assess the RoF systems is error vector magnitude (EVM) measurement; BER could be estimated according to EVM reading.

2. Mobile Fronthaul under Investigation

A schematic diagram of the single-optical channel MFH under observation is depicted in Fig. 2a. Block diagrams related to the BBU, optical fiber link, and RRU are illustrated in Fig. 2b-d, respectively. In the BBU, multiple intermediate frequency (IF) technique is used to aggregate many modulated mobile signals. OFDM technique is used to map the data of one baseband mobile signal. Each of the resultant OFDM signal is used to modulate one of the RF (i.e., IF) carriers. The modulated RF carriers are multiplexed and the resultant waveform is applied to a digital-to-analog convertor (DAC). The generated analog signal is then mapped on the semiconductor laser optical carrier using analog optical intensity modulator. (See Fig. 2b). Few

remarks related to the MFH transmitter are given in the following

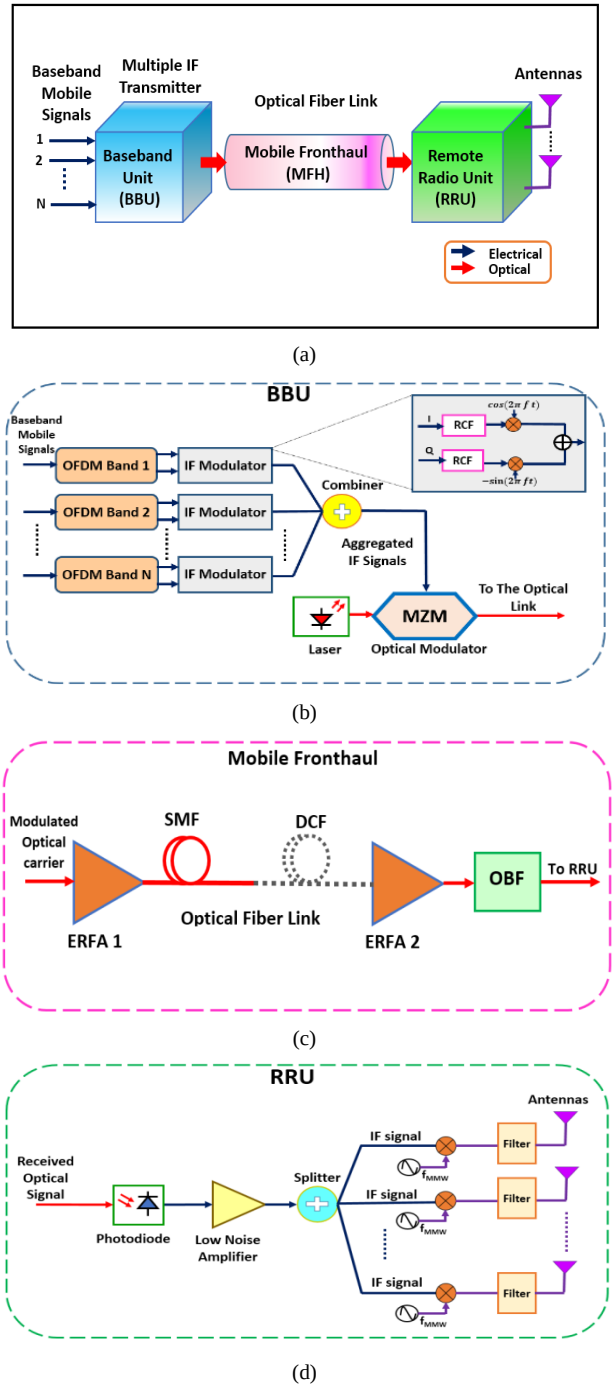

Figure 2. (a) Schematic diagram of single-optical channel mobile fronthaul. (b) Block diagram of the baseband unit (insert represents signal shaping with raised-cosine filter then mapped on IF carrier). (c) Block diagram of the optical fiber link. (d) Block diagram of the remote radio unit

1. Direct detection (DD)-OFDM technique is adopted to map the baseband mobile signal on the IF carrier. The OFDM technique offers about 50% spectral efficiency with reduced channel equalization requirement [63, 64]. Further, DD-OFDM is less expensive compared with coherent (CO)-OFDM. Recently, 200 Gb/s DD-OFDM has been demonstrated experimentally [65].
2. High-order modulation formats such as QPSK, 16QAM and 64QAM are used with the DD-OFDM to achieve high spectral efficiency.
3. Raised-cosine filter (RCF) is used to shape each of the modulated IF carrier to achieve negligible inter-symbol interference (ISI) at the receiver detection process. For a RCF roll-off factor equals r, the transmitted bit rate of each mobile signal is given by

$$B_r = \frac{2m\,B_{ch}}{(1+r)} \quad (1)$$

where B_{ch} is the mobile channel bandwidth and $m = \log_2 M$ is the order of the modulation (M is the number of discrete symbols). In writing eqn. 1, it is assumed that the electrical OFDM offers 50% spectral efficiency and B_{ch} corresponds to a double-sideband spectrum around each IF carrier.

4. The radio intermediate frequencies (f_n, n= 1, 2…N, with N is the number of aggregated mobile signals) are equally spaced with channel spacing $\Delta f_{IF} \equiv f_{n+1} - f_n \geq B_{ch}$. The composite electrical signal (i.e., multiple IF signal) applied to the optical modulator can be considered as an effective baseband RF signal covers the spectrum extending from $f_1 - B_{ch}/2$ to $f_N + B_{ch}/2$ which corresponds to a frequency band of $(f_N - f_1) + B_{ch} = (N-1)\,\Delta f_{IF} + B_{ch}$ (see Fig. 3). Thus the effective baseband RF signal bandwidth (measured from f = 0) is given by

$$B_{eff} = f_1 + \frac{B_{ch}}{2} + (N-1)\,\Delta f_{IF} = f_N + \frac{B_{ch}}{2} \quad (2)$$

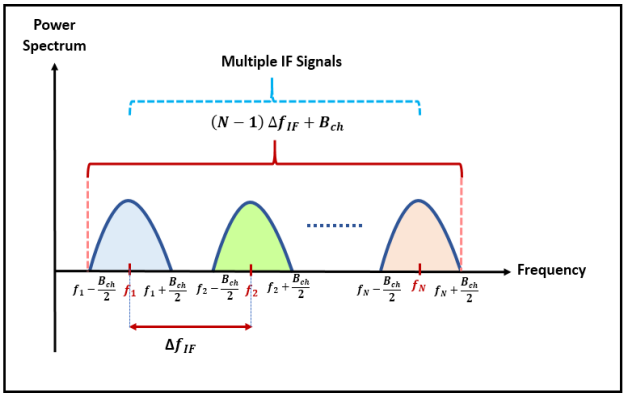

Figure 3. Effective bandwidth of aggregated baseband IF signals

5. MMW photonic generation may be used to shift the spectrum of the multiple IF signal around the required MMW carrier at the receiver side. This is achieved using photonic mixing technique in the photodiode [66-68]. In this case the modulated optical carrier is combined with the output of a continuous wave (CW) (i.e., unmodulated) semiconductor laser at the fiber input. The optical carrier frequency f_{O1} and the CW laser f_{O2} is chosen according to the required MMW carrier frequency, f_{MMW} [67]

$$f_{MMW} \equiv f_{O1} - f_{O2} \approx \frac{c}{\lambda_{O1}^2} \quad \Delta \qquad (3)$$

where c is the speed of light in free space and $\Delta\lambda$ is the wavelength separation between the two lasers wavelengths.

6. An external optical modulator is used in this work since it is suitable for high speed operation with little chirp effect compared with the internal optical modulator [59]. The external modulator is designed used Mach-Zehnder configuration.

The optical link consists of two erbium-doped fiber amplifiers (EDFAs), a single-mode fiber (SMF), and an optical bandpass filter (OBF), see Fig. 2c. The first EDFA acts as an optical amplifier (OA) to boost the power of the modulated carrier. The second EDFA is used to compensate the fiber loss. The OBF is used to suppress the amount of amplified spontaneous emission noise, generated by the OAs, that incidents on the photodiode. The SMF is characterized by four parameters: length L_{SMF}, attenuation α_{SMF}, chromatic (group-velocity) dispersion D_{SMF}, and dispersion slope S_{SMF}. At 1550 nm (i.e., minimum fiber attenuation wavelength), α_{SMF} = 0.2 dB/km, D_{SMF} = 16.75 ps/(nm.km), and S_{SMF} = 0.075 ps/(nm^2.km). At 1310 nm wavelength (i.e., zero fiber group-velocity dispersion (GVD) wavelength), α_{SMF} = 0.34 dB/km, D_{SMF} = 0, and S_{SMF} = 0.0856 ps/(nm^2.km). The gain of the second OA (in decibel) is set equal (α_{SMF} L_{SMF}).

The high GVD of the SMF at 1550 nm limits the maximum allowable transmission distance at high bit rate when the system operates at this wavelength. To compensate the effect of GVD, a dispersion-compensation fiber (DCF) having high negative GVD at 1550 nm is connected at the end of the SMF section. The length of the DCF, L_{DCF}, is chosen to yield a negligible total GVD over the fiber link.

$$D_{DCF} = -(L_{SMF}/L_{DCF})\, D_{SMF} \qquad (4)$$

At 1550 nm, the DCF used in this work has α_{DCF} = 0.6 dB/km, D_{DCF} = -80 ps/(nm.km), and S_{DCF} = -0.075 ps/(nm^2.km). When a DCF is used in the link, the gain at the second OA is raised to (α_{SMF} L_{SMF} + α_{DCF} L_{DCF}).

The optical bandpass filter has a center frequency that matches the optical carrier frequency $f_O = c/\lambda$ and a bandwidth suitable for passing the two side bands (upper and lower) associated with the modulated optical carrier. Thus the OBF should be at least equal $2B_{eff}$ with careful attenuation should be paid to ensure that the lasing frequency of the CW laser (if used) should be within the filter spectrum.

At the remote radio unit side, the modulated optical carrier is applied to a PIN photodiode. The resultant photocurrent has the modulated signal spectrum centered at the required MMW carrier. The photocurrent is amplified using low-noise wideband amplifier and then distributed to the MMW transmitter antennas as shown in Fig. 2d.

3. Simulation Results

Simulation results are presented for two values of mobile channel bandwidth, B_{ch} = 200 MHz (case I) and 1 GHz (case II). The first case covers services when one goes smoothing from LTE-A to 5G mobile systems. The second case is useful to estimate the performance of broadband RoF-based 5G mobile system which is expected to cover different applications in the next future. For each case, four scenarios are investigated as follows

Scenario 1: The system operates at 1550 nm wavelength using SMF link.

Scenario 2: The system operates at 1310 nm wavelength using SMF link.

Scenario 3: As in Scenario 1, but a DCF is used to compensate the GVD of the SMF.

Scenario 4: WDM technique is used in the 1550 nm band with a SMF-based link.

Table 1 lists the bit rates corresponding to both cases when different modulation formats are used. The results are obtained from eqn. (5) using r = 0.25.

$$B_r = 2B_{ch}\log_2(M)/(1+r) \qquad (5)$$

Table 1. Bit rates corresponding to mobile channel bandwidth of 200 MHz and 1 GHz assuming r= 0.25

Modulation Format	Bit Rate (Gb/s)	
	B_{ch} = 200 MHz	B_{ch} = 1 GHz
BPSK	0.320	1.6
QPSK	0.640	3.2
16QAM	1.28	6.4
32QAM	1.60	8
64QAM	1.92	9.6

The simulation results are obtained using a commercial software package, namely Optisystem V.14.1. Unless otherwise stated, the parameter values used in the simulation are listed in Table 2. In these results, the maximum transmission distance for a given transmitter laser launch power is estimated to yield the maximum allowable error vector magnitude (EVM). The maximum allowable EVM, EVM_{max}, is taken to be 17.5, 12.5, and 8% for QPSK, 16QAM, and 64QAM, respectively [69]. The corresponding bit error rate (BER) threshold is equals to 5.5x10^{-9}, 1.3x10^{-4}, and 2x10^{-3}, respectively, and it is estimated using the following equation [70]

$$BER = \frac{4(1-M^{-1/2})}{\log_2 M} Q\left[\sqrt{\frac{3}{EVM^2\,(M-1)}}\right] \qquad (6)$$

where M is order of the *M*-ary modulation format (taken to be one dimension) and Q[.] is the Q-Function.

3.1. Case I: 200 MHz-Mobile Channel Bandwidth

Consider first the transmission of 5G services over a single carrier of 1550 or 1310 nm wavelength. The optical transmitter can be considered as a multiband optical OFDM where each OFDM, which corresponds to one of the baseband mobile signals, is mapped on a specific IF (i.e., RF carrier). The frequency of the n*th* subcarrier is set to 0.35n

GHz to yield a frequency guard band between successive channels.

Figures 4 and 5 show examples of the obtained waveforms corresponding to the transmission of 16x200 MHz- mobile signals over a SMF at 1550 nm wavelength. The results are obtained for -4 dBm launch laser power and 16QAM signaling format. This format yields a bit rate of 1.28 Gb/s per baseband mobile signal (see Table 1). Figure 4 contains several parts describing the RF spectrum of the 16 aggregated signals for different cases. Part a of Fig. 4 illustrates the spectrum of aggregated carriers (ACs) at the transmitter side (used to modulate the intensity of the optical carrier). Parts b-e of the figure show the detected RF spectrum at the receiver end (after the photodiode (PD)) after different transmission lengths over the SMF (back-to-back (B2B), 30, 40 and 50 km, respectively). For comparison purposes, two additional parts (f and g) are given in this figure. Part f displays the detected RF spectrum after 50 km transmission when the system operates at 1310 nm (corresponding to zero GVD of the standard SMF). Part g gives the results corresponding to the transmission over 50-km SMF at 1550 nm when DCF is employed. Investigating the results in Fig. 4 reveals the key role played by the 1550-nm GVD on degraded system performance. Note that the power degradation increases with channel index (i.e., IF carrier frequency). This results is expected since the baseband version of the SMF transfer function has a lowpass characteristics.

For a fixed fiber lengths L, the power of the transmitted RF signal will be vanished at discrete frequencies f_{zero} given by [71]

$$f_{zero} = \left(\frac{Jc}{2\lambda^2 DL}\right)^{1/2} \quad (7)$$

where J is an integer. The lowest value of f_{zero} occurs at J=1 and estimated to be 13.65, 11.14, 9.65, 8.63 and 7.88 GHz when SMF of length 20, 30, 40, 50 and 60 km, respectively, is used at 1550 nm transmission wavelength. The presence of f_{zero} becomes clear as the number of aggregated channels N increases. This is clear in Fig. 5 which shows the detected spectrum at the fiber end when 48 signals are transmitted with P_T = -3 dBm and 16QAM format.

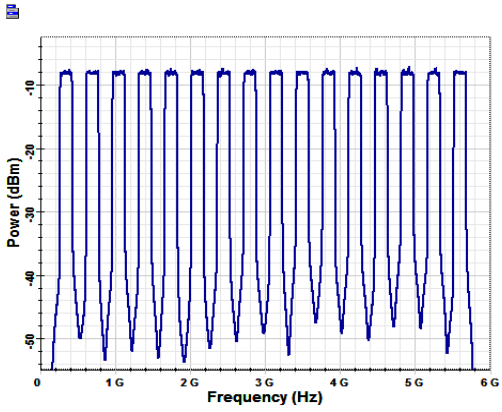

(a)

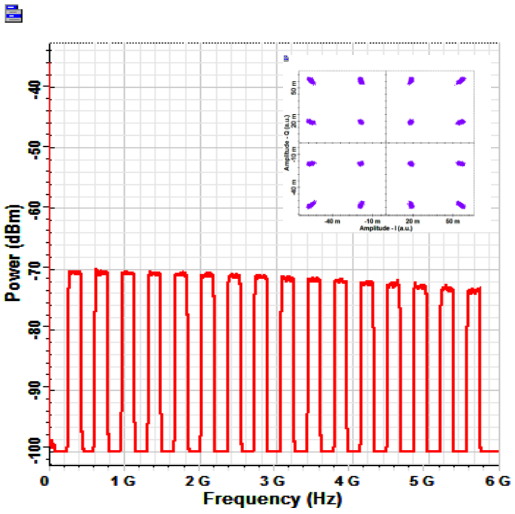

(b)

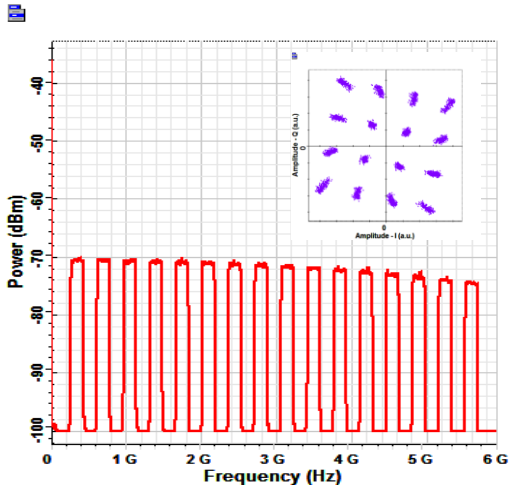

(c)

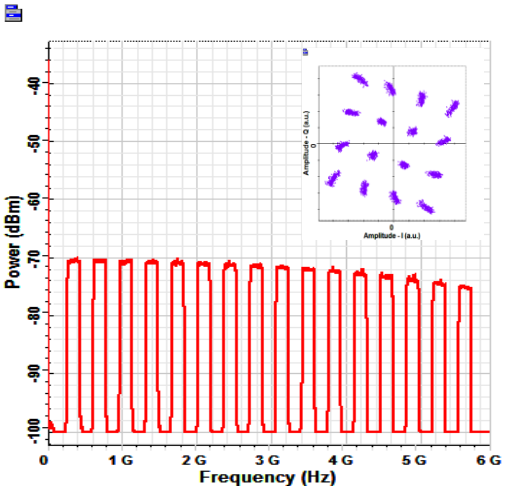

(d)

Figure 4. Electrical spectrum of aggregated 16x200 MHz 16QAM signals (a) At the transmitter side. (b-e) Detected spectra after B2B, 30, 40, 50 km SMF transmission at 1550 nm, respectively. (f) Detected spectrum after 50 km SMF at 1310 nm. (g) Detected spectrum after 50 km SMF+DCF at 1550 nm. The inserts in parts (b-g) represent constellation diagram

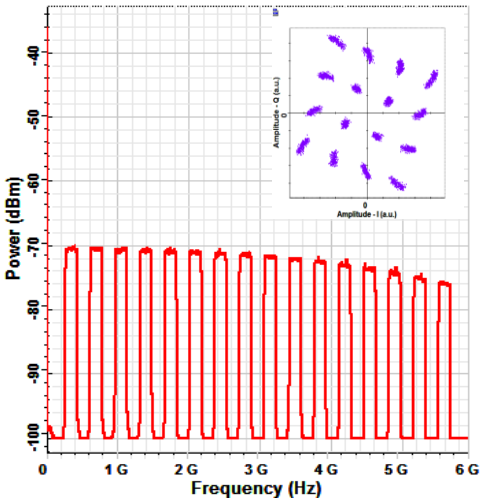

(e)

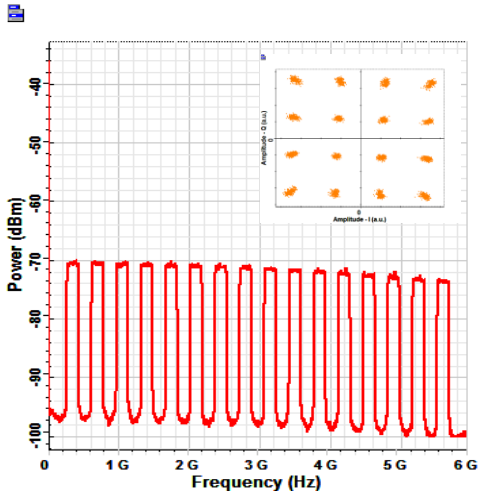

(f)

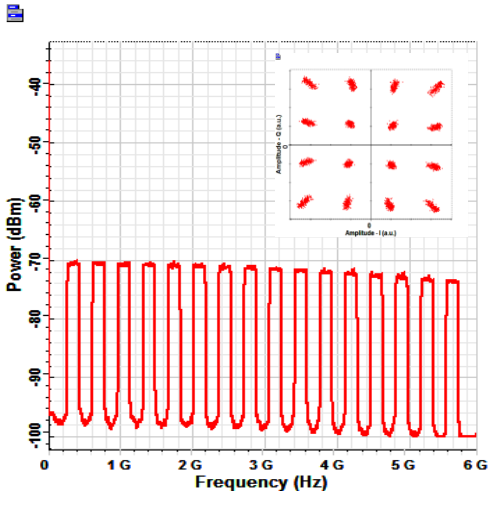

(g)

Figure 4. Cont.

Table 2. Parameters values used in the simulation

Unit	Subunit	Parameter	Value
Baseband Unit (BBU)	OFDM Modulator	Number of Subcarrier Cyclic Prefix Average OFDM Power	512 0 16 dB
	Transmitter Laser	Wavelength Power Line width	1550 or 1310 nm -4 to 4 dBm 0.1 MHz
	Optical Modulator (Analog Intensity MZM)	Insertion Loss Switching Bias Voltage Switching RF Voltage Extinction Ratio	2 dB 4 V 4 V 30 dB
Optical Link	EDFA 1	Gain Noise Figure	6 dB 4 dB
	Standard Single Mode Fiber (SMF)	Wavelength Attenuation Dispersion Dispersion Slop Polarization Dispersion	1550, 1310 nm 0.2, 0.34 dB/km 16.75, 0 ps/(nm.km) 0.075, 0.0856 ps/(nm^2.km) 0.05 ps/km^{½}
	Dispersion Compensation Fiber	Wavelength Attenuation Dispersion Dispersion Slop Polarization Dispersion	1550 nm 0.6 dB/km -80 ps/(nm.km) -0.075 ps/(nm^2.km) 0.5 ps/km^{½}
	EDFA 2	Gain Noise Figure	Depend on fiber length 4 dB
	Optical Bandpass Filter	Center Frequency Bandwidth	Equal to optical carrier (f_o) $2xB_{eff}$
Remote Radio Unit (RRU)	PIN Photodiode Receiver	PD Responsively Center Frequency	1 A/W Optical carrier frequency

Figure 6 shows the signal spectrum at different points of the system when 16x200 MHz signals are aggregated. The results correspond to 1550 nm system operating with 10 km-SMF P_T = -4 dBm and 16QAM format. The spectrum in part a of this figure is for the first IF carrier (f1= 0.35 GHz). Note that the optical distortion level is about 56 dB lower than the signal level. This gives clear indication of the linearity of the MZM used in the simulation.

The variation of the EVM with channel index n and launch power P_T is also estimated for 16QAM signaling and λ=1550 nm and the results are shown in Figs. 7 a-c for number of aggregated carriers N=16, 32 and 48 at distances 30, 6, and 3 km, respectively. These distances are chosen to avoid exceeding EVM_{th}= 12.5% by the aggregated carriers. Note that at specific P_T, the value of EVM generally increases with channel index. This indicates clearly that the high-index channel should be kept under observation during test.

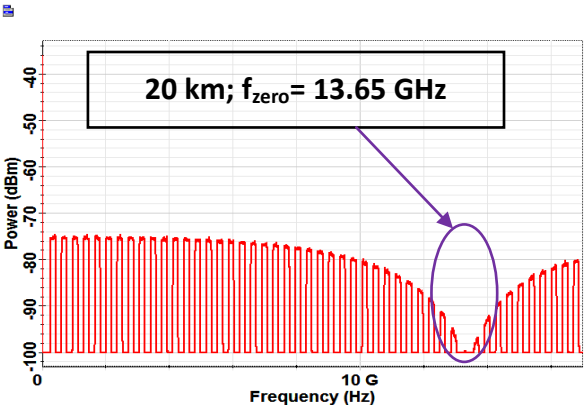

(a)

Figure 5. Detected spectrum corresponding to the transmission of 48x200 MHz-channel bandwidth 16QAM at P_T = -3 dBm over SMF-1550 nm (a) 20 km (b) 30 km (c) 40 km (d) 50 km (e) 60 km

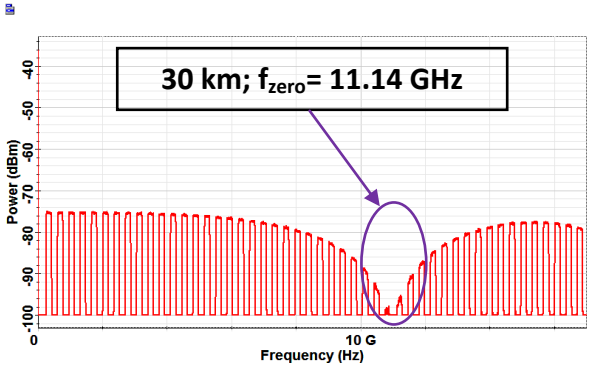

(b)

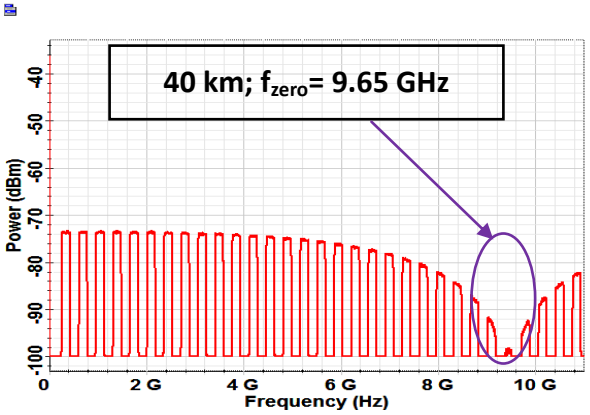

(c)

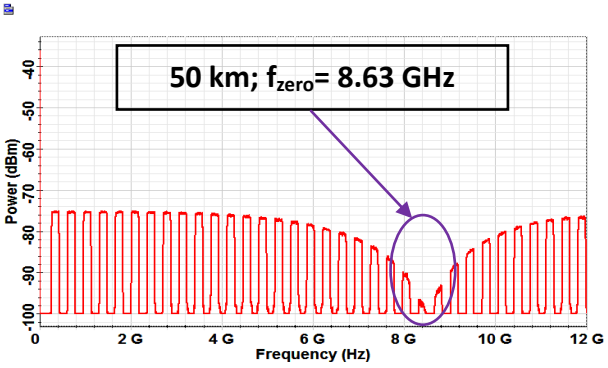

(d)

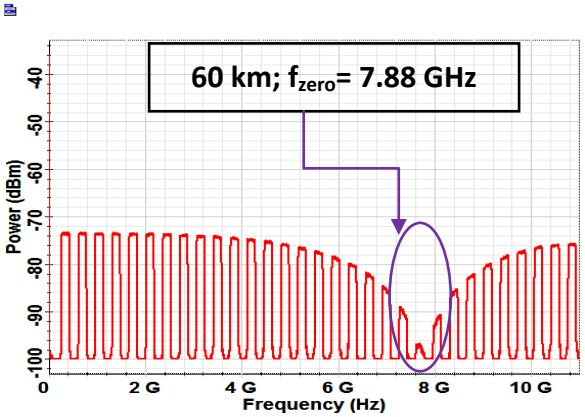

(e)

Figure 5. Cont.

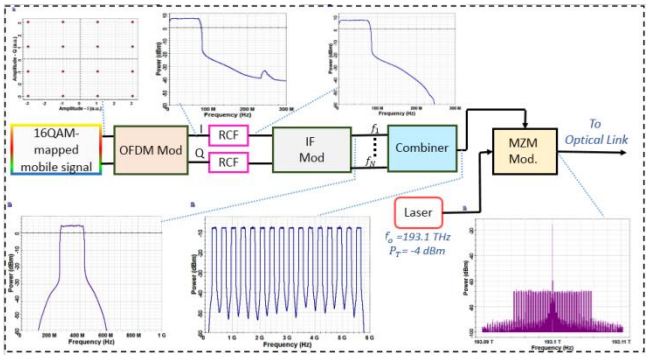

(a)

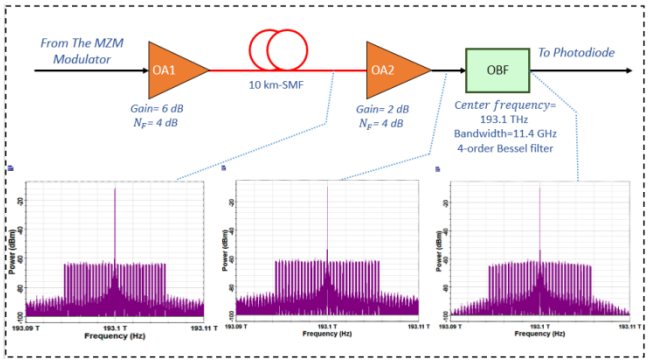

(b)

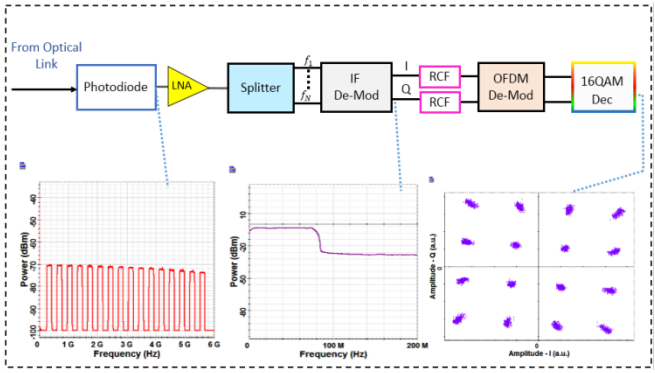

(c)

Figure 6. Spectrum at different points of the system when 16x200 MHz signals are aggregated and correspond to 1550 nm system operating with 10 km-SMF and 16QAM OFDM P_T = -4 dBm. (a) Transmitter side. (b) Optical fiber link. (c) Receiver side

The simulation is carried further to estimate the effect of transmission distance on the EVM. The results are depicted in Figs. 8 a-c for N=16, 32 and 48, respectively. The results are obtained for SMF link at 1550 nm wavelength and system operates with 16QAM signaling and different launch power. These figures are used to estimate the maximum allowable transmission length L_{max} at which EVM becomes equal its threshold value, EVM_{th} = 12.5%. At given P_T, channel index, and transmission length L, EVM is an increasing function of N. For examples at P_T = -3dBm and L= 3 km, EVM equals 8.9, 9.7 and 12.5 when N = 16, 32 and 48. These values are to be compared with 5.4, 5.9 and 8.0, respectively, when P_T increase to 0 dBm and keeping L at the same value.

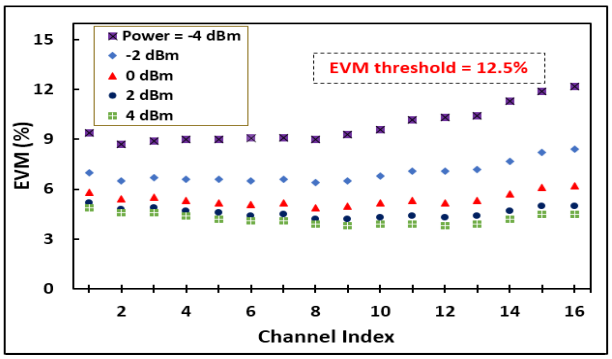

(a)

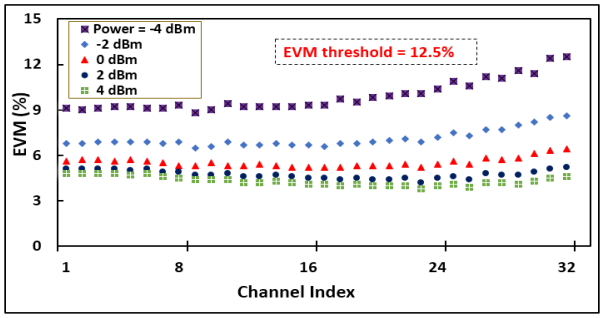

(b)

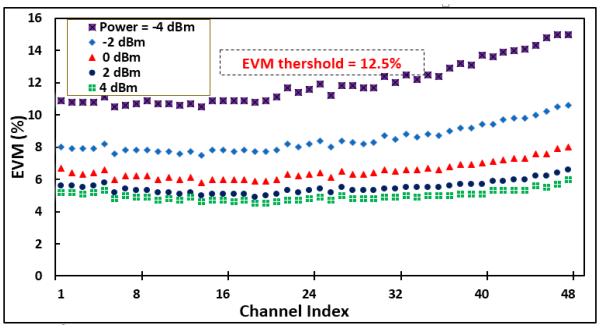

(c)

Figure 7. EVM as a function of channel index n with various levels of launch power for aggregated 200 MHz 16QAM mobile signals transmitted over a SMF at 1550 nm (a) N= 16 at 30 km. (b) N= 32 at 6 km. (c) N=48 at 3 km

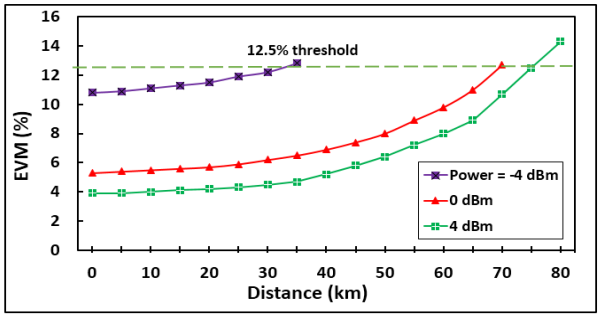

(a)

Figure 8. Dependence of error vector magnitude on the lengths of the SMF link at 1550 nm operating wavelength and for aggregated N channels of 200 MHz 16QAM at different levels of launch power (a) N= 16. (b) N= 32. (c) N= 48

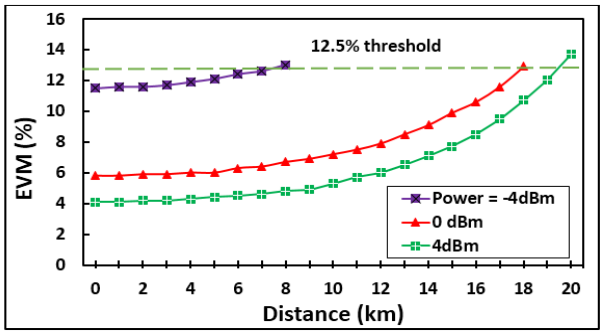

(b)

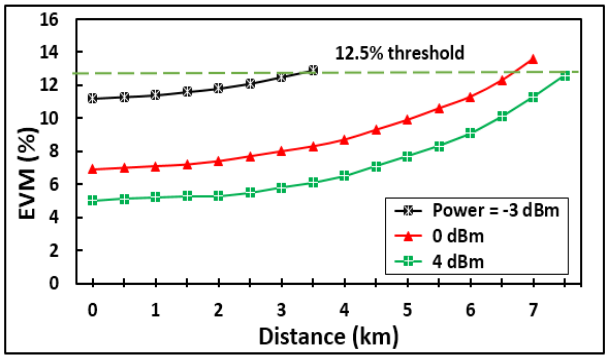

(c)

Figure 8. Cont.

Tables 3a-c present the dependence of maximum transmission distance on the transmitter laser power P_T for QPSK, 16QAM, and 64QAM, respectively. The results are given for 1550 nm system incorporating a SMF link and for three values of number of aggregated mobile signals, N= 16, 32, and 48. Investigating the results in Table 3 reveals the following findings

1. In the case of QPSK signaling, increasing the number of aggregated channels from 16 to 32 and 48 will reduce the maximum transmission distance by 25% and 10%, respectively. These values are to be compared with 25% and 8%, respectively, for 16QAM signaling and 30% and 17%, respectively, for 64QAM signaling.
2. Increasing P_T leads to increase in L_{max} till a saturation level is reached. For example, L_{max} saturates approximately at 89 km when P_T equals 4 dBm for N=16. Using N=32 (48) will make L_{max} goes to 22 km (9 km) when P_T tends to 2 dBm.
3. The maximum transmission distance is a decreasing function of both modulation order and number of aggregated channels N. for example, using P_T = 0 dBm and N=16 give L_{max} = 82, 69, and 25 km for QPSK, 16QAM, and 64QAM, respectively. These values are to be compared with 21, 17, and 7 km, respectively, when N increases to 32. Increasing N further to 48 yields L_{max} of 8, 6, and 4 km, respectively.

Table 3. Maximum transmission distance for various transmitter launch power, number of 200 MHz-aggregated mobile channels, and modulation formats

(a) QPSK

Launch power (dBm)	Maximum distance (km)		
	16 channels	32 channels	48 channels
-4	65	16	5
-3	70	18	7
-2	75	20	7
-1	80	21	8
0	82	21	8
1	85	22	8
2	87	22	9
3	88	22	9
4	89	22	9

(b) 16QAM

Launch power (dBm)	Maximum distance (km)		
	16 channels	32 channels	48 channels
-4	30	6	--
-3	50	12	3
-2	55	14	4
-1	65	16	5
0	69	17	6
1	71	18	6
2	73	18	7
3	75	19	7
4	75	19	7

(c) 64QAM

Launch power (dBm)	Maximum distance (km)		
	16 channels	32 channels	48 channels
-4	--	--	--
-3	--	--	--
-2	--	--	--
-1	10	4	2
0	25	7	4
1	30	10	5
2	35	12	6
3	35	13	6
4	35	13	6

Table 4 compares the performance of the system for three link scenarios (SMF at 1550 nm, SMF at 1310 nm, and SMF with DCF at 1550 nm). Low values of P_T are used in this table to highlight the possibility to go to green-communication environment with 5G transmission system. The results are displayed for three modulated formats (QPSK, 16QAM, and 64QAM) and assuming that the system deals with N=16, 32, and 48. Note that the QPSK signal gives practical transmission distance with P_T = -4 dBm for all values of N considered here. In contrast, using 16QAM signaling with SMF at 1550 nm, P_T = -4 dBm doesn't give satisfactory results when N=48 and therefore, P_T increases to -3 dBm for this case. The simulation also indicates that P_T less than -1 dBm doesn't give practical results when 64 QAM signaling is used with the SMF at 1550 nm. The results in Table 4 highlights two facts

1. The maximum transmission distance obtained with Scenario 2 (SMF+1310 nm) and Scenario 3 (SMF+DCF+1550 nm) is almost the same.
2. The effect of operating at 1310 nm or at 1550 nm with dispersion compensation is more pronounced for increasing L_{max} when N increases. For example $(L_{max})_2/(L_{max})_1$ = 1.15, 4.06, and 10.00 when N=16, 32, and 48. These values are to be compared with $(L_{max})_3/(L_{max})_1$ = 1.15, 4.06, and 8.00, respectively. Here the subscripts 1, 2, and 3 refer to the scenario number. The enhancement in the transmission distance achieved by using Scenario 2 and 3 over Scenario 1 is listed in Table 5.

Table 4. Variation of maximum transmission distance for the three operating scenarios assuming 200 MHz-bandwidth mobile signals

Modulation Format	Number of Channels	Launch Power (dBm)	$(L_{max})_2/(L_{max})_1$	$(L_{max})_3/(L_{max})_1$
QPSK	16	-4	1.15	1.15
	32	-4	4.06	4.06
	48	-4	10.00	8.00
16QAM	16	-4	1.67	1.50
	32	-4	5.00	4.17
	48	-3	10.00	8.33
64QAM	16	-1	2.00	2.00
	32	-1	2.50	2.50
	48	-1	5.00	5.00

Table 5. Maximum transmission distance enhancement achieved by using Scenario 2 (SMF 1310 nm) and Scenario 3 (SMF+DCF 1550 nm) over Scenario 1 (SMF 1550 nm) assuming 200 MHz-mobile channel bandwidth

No. of Channels	Modulation Format	Launch Power (dBm)	Maximum Distance (km)		
			SMF 1550 nm	SMF 1310 nm	SMF+DCF 1550 nm
16	QPSK	-4	65	75	75
32		-4	16	65	65
48		-4	5	50	40
16	16QAM	-4	30	50	45
32		-4	6	30	25
48		-3	3	30	25
16	64QAM	-1	10	20	20
32		-1	4	10	10
48		-1	2	10	10

We carry the simulation further to investigate the use of WDM technique to increase the number of transmitted mobile channels over the optical link. As an example, the transmission of 48 mobile signals using three-optical channel WDM system operating in the C-band region is considered here. Three semiconductor lasers are used in the transmitter side emitting at 193.05, 193.1, and 193.15 THz (i.e. 50 GHz channel spacing) according to International Telecommunication Union (ITU-U) grid. Each laser is modulated by 16 aggregated baseband mobile signals using 16QAM modulation format. Figure 9a shows the optical

spectrum of the WDM signal at the fiber input. Figure 9b depicts the variation of EVM with channel index when SMF is used with P_T = -4 dBm. Note that the dependence of EVM on channel index gives the same behavior for each one of the WDM channels. The simulation results of 48 channels reveal that using P_T = -4 dBm gives L_{max} of 60 and 30 km when QPSK and 16QAM signaling formats are used, respectively. These values are to be compared with 65 and 30 km, respectively when 16 channels are transmitted over a single optical carrier.

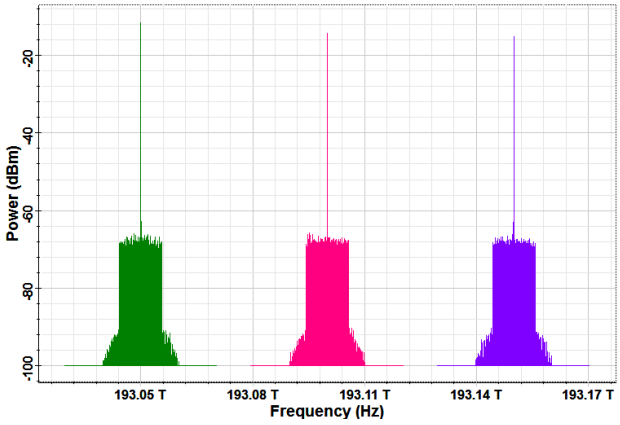

(a)

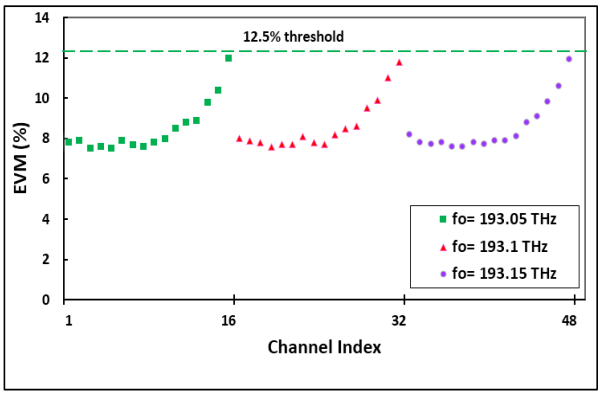

(b)

Figure 9. Simulation results related to a 3-channel C-band WDM system operating at P_T = -4dBm. Each optical carrier is modulated by 16x200 MHz 16QAM signals (a) Optical spectrum at the fiber input. (b) Error vector magnitude after 30 km –transmission

3.2. Case II: 1GHz-Mobile Channel Bandwidth

Future applications of 5G system requires high-data rate services which can be incorporated using wide baseband mobile signals (i.e., wide mobile channels B_{ch}) supported by high-order modulation. In this subsection, simulation results are presented for B_{ch} = 1 GHz. In this case, the baseband mobile signal carries 3.2, 6.4, and 9.6 Gb/s when QPSK, 16QAM, and 64 QAM signaling are used, respectively. As expected, the effect of GVD of the 1550 nm SMF link is more pronounced with B_{ch} = 1 GHz compared with B_{ch} = 200 MHz under the assumption of equal number of aggregated IF carriers *N*. Therefore, WDM technique can be used here to reduce the effect of fiber dispersion when large number of wide mobile signals are aggregated. The solution is achieved by dividing the *N* IF carriers into groups and each group is used to modulate an optical carrier emitted by one of the WDM transmitter lasers. In this subsection, the key role played by the WDM technology on the transmission performance of aggregated 1 GHz mobile signals over a SMF is also investigated. Summary of the simulated results related to the maximum transmission distance are given here. The signal waveforms and spectra are given in Appendix A. The results are reported for 1.15 GHz IF channel spacing and the n*th* IF carrier frequency is set equal 1.15n GHz.

Table 6 lists the maximum allowable transmission length L_{max} for Scenario 1 assuming a single-optical carrier and eight aggregated signals (N=8). The values of L_{max} are given for different transmitter laser power P_T and for three modulated formats (QPSK, 16QAM and 64QAM). Results related to P_T less than -2 dBm for 16QAM and less than -1 dBm for 64 QAM are not reported here since the obtained EVM in the simulation exceeds the EVM threshold when B2B transmission is considered. Note that the 8-channel QPSK system offers a maximum transmission length of 26 km when P_T = -1 dBm. This value is to be compared with 17 and 5 km when 16QAM and 64 QAM formats are used, respectively. The relative transmission distances $(L_{max})_{16QAM}/(L_{max})_{QPSK}$ and $(L_{max})_{64QAM}/(L_{max})_{QPSK}$ are 0.65 and 0.19, respectively. Increasing P_T will enhance the maximum transmission distance but with almost saturation behavior which is more pronounced for low-order modulation format. For example, increasing P_T to 0 dBm gives L_{max}= 29, 20, and 13 km for QPSK, 16QAM, and 64QAM system, respectively. These values give $(L_{max})_{16QAM}/(L_{max})_{QPSK}$ = 0.69 and $(L_{max})_{64QAM}/(L_{max})_{QPSK}$ = 0.45. At P_T = 4 dBm, the relative transmission distances of 16QAM and 64QAM over QPSK are 0.80 and 0.7, respectively. Note also that L_{max} approaches a saturated level of approximately 30 km when P_T exceeds -1 dBm for QPSK format is used. This value is to be compared with 24 km at P_T = 3 dBm for 16QAM format and 21 km at P_T = 4 dBm for 64QAM format.

It is clear from the previous results that the GVD of SMF-based system operating at 1550 nm limits the maximum transmission distance to about 30, 24, and 21 km when QPSK, 16QAM, and 64QAM are used, respectively, with N=8. To reduce the effect of GVD, one can go to Scenario 2 or 3 to increase the transmission distance as shown in Table 7. The results in this table are presented for QPSK, 16QAM, and 64QAM system operating with minimum launch power (P_T = -4, -2, and -1dBm, respectively). At these values of P_T, Scenario 1 yields 15, 12, and 5 km for the three modulation formats, respectively. Note that Scenario 2 enhances the maximum transmission distance by 3.67, 3.75, and 5.00 when QPSK, 16QAM, and 64QAM formats are used, respectively, note also Scenario 3 gives transmission enhancement of 2.66, 2.08, and 3.00, respectively. It's clear that operating with Scenario 2 or 3 is

most effective in the 64 QAM system since the impact of GVD on transmission performance of the system is the highest compared with QPSK and 16QAM systems.

Table 6. Maximum distances as a function of launch power for various modulation formats assuming 8x1 GHz-bandwidth mobile signals

Launch Power (dBm)	Maximum Distance (km)		
	QPSK	16QAM	64QAM
-4	15	--	--
-3	20	--	--
-2	23	12	--
-1	26	17	5
0	29	20	13
1	29	22	17
2	29	23	19
3	29	24	20
4	30	24	21

Table 7. Maximum transmission distance for the three operating scenarios using 1 GHz-bandwidth mobile signals

Modulation Format	Launch Power (dBm)	Distance (km)		
		SMF 1550 nm	SMF 1310 nm	SMF+DCF 1550 nm
QPSK	-4	15	55	40
16QAM	-2	12	45	25
64QAM	-1	5	25	15

Table 8. Effect of number of WDM channels on maximum transmission distance. Each optical channel is modulated by 8x1 GHz-bandwidth mobile signals mapped with 64QAM format

Launch power (dBm)	Maximum Distance (km)		
	Single Optical Channel	Eight Optical Channels	Sixteen Optical Channels
-1	5	2	--
0	13	7	5
1	17	12	10
2	19	15	10
3	20	16	10
4	21	16	10

The next step in the simulation is directed toward using WDM technique to enhance the transmission capacity of 5G services over the fiber. The results are presented here for the case of transmission 8x1 GHz-bandwidth mobile signal per a single-optical carrier using 64QAM signaling. The 64QAM formats offers the highest transmission bit rates compared with other formats considered in this paper but also characterized by worst performance degradation due to GVD. Table 8 lists the maximum transmission distance over a SMF when the system operates with single (bit rate=76.8 Gb/s), eight (bit rate=614.4 Gb/s), and sixteen optical channels (bit rate=1.228 Tb/s). The operating frequency of the transmitter laser are selected to be in the C-band (1550 nm window) with 50 GHz-channel spacing according to IUT grid. At $P_T = 0$ dBm, L_{max} reduces from 13 km in the case of using a single-optical channel to 7 km and 5 km for 8-cahnnel and 16-channel WDM systems, respectively. With $P_T = 4$ dBm, L_{max} approaches a saturation level of 21, 16, and 10 km when WDM is designed with single, eight, and sixteen optical channel, respectively. This indicates that L_{max} reduces by about 0.75 and 0.5 when eight and sixteen optical channels are used, respectively.

4. Conclusions

The dependence of maximum transmission distance L_{max} of analog RoF-based MFH on number of aggregated IF carriers N, mobile baseband bandwidth B_{ch}, and modulation format has been estimated for 5G mobile network. Results have been reported for two values of B_{ch}, 200 and 1000 MHz, and for four SMF-link scenarios (1550 nm, 1310 nm, 1550 nm with DCF, and C-band WDM). The main calculations drawn for this study are

1. Using $B_{ch} = 200$ MHz, $P_T = 0$ dBm, N= 16, and 1550 nm SMF yields $L_{max} = 82$, 69, and 25 km for QPSK, 16QAM, and 64QAM, respectively. These values are to be compared with (21, 17, and 7 km) and (8, 6, and 4 km) when N increases to 32 and 48, respectively. The increase in L_{max} through the operation at 1310 nm or 1550 nm with DCF is more pronounced with increasing N. operating at 1310 nm enhance L_{max} by 1.15, 4.06, and 10.00 when N= 16, 32, and 48 are used with 16QAM signaling.
2. Using WDM technique can enhance the capacity of MFH with negligible effect on L_{max} when 200 MHz signals are aggregated. In contrast, WDM is associated with reduced L_{max} when B_{ch} increases to 1 GHz. The value of L_{max} reduces from 13 to 7 and 5 km when the number of multiplexed optical channels increase from 1 to 8 and 16, respectively, under the assumption of transmission over a SMF using 64QAM, 8 mobile signals per optical carrier and $P_T = 0$ dBm.

ACKNOWLEDGEMENTS

One of the authors, S. S. Jawad, acknowledges the Iraqi Ministry of Youth and Sport for offering M.Sc scholarship to do this work at Al-Nahrain University.

Appendix

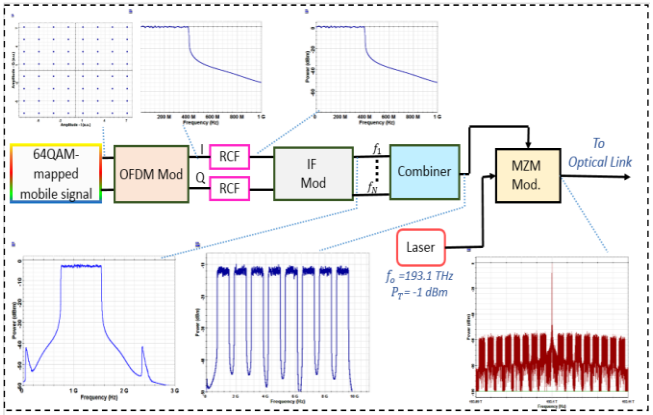

(a)

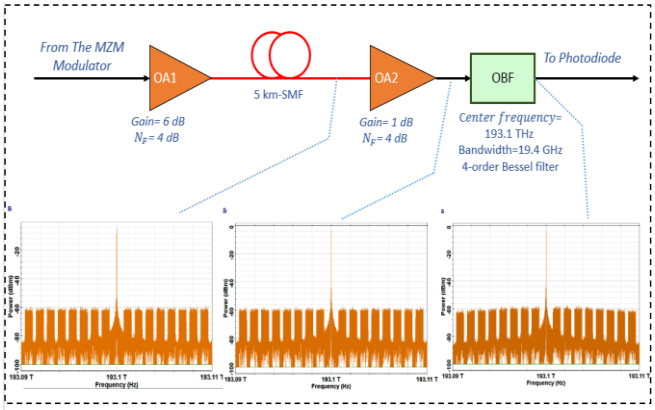

(b)

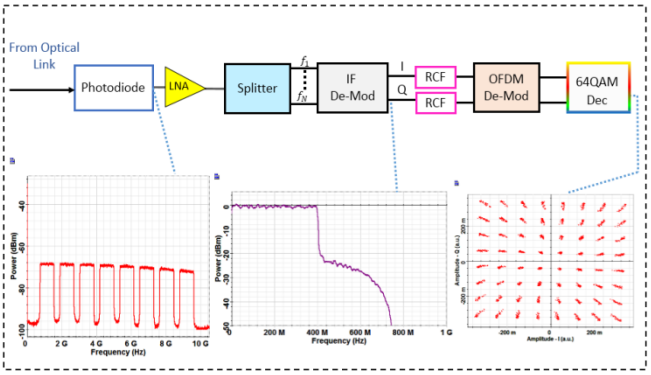

(c)

Figure 10. Spectrum at different points of the system when 8x1 GHz signals are aggregated and correspond to 1550 nm system operating with 5 km-SMF and 64QAM OFDM P_T = -1 dBm. (a) Transmitter side. (b) Optical fiber link. (c) Receiver side

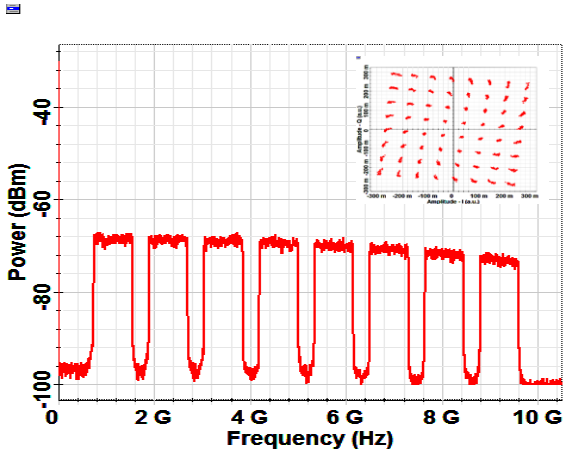

(a)

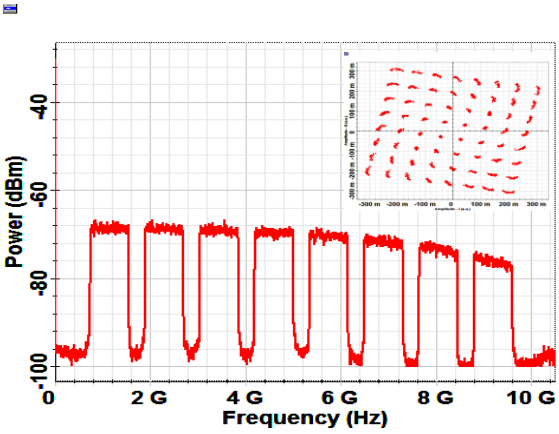

(b)

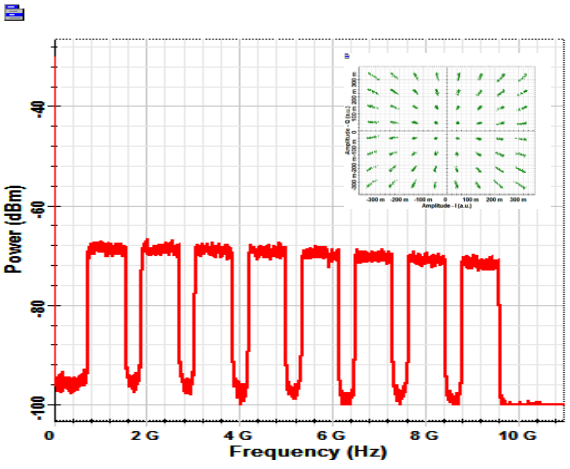

(c)

Figure 11. Detected spectra of aggregated 8x1 GHz-mobile signals corresponding to at P_T = -1 dBm and 64QAM format with (a) 15km-SMF at 1550 nm. (b) 25 km-SMF at 1550 nm. (c) 25 km-SMF at 1310 nm. (d) 15 km-SMF+DCF at 1550 nm. Inserts represent constellation diagram

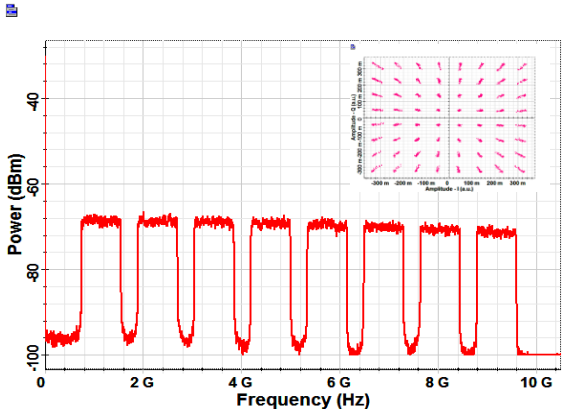

(d)

Figure 11. Cont.

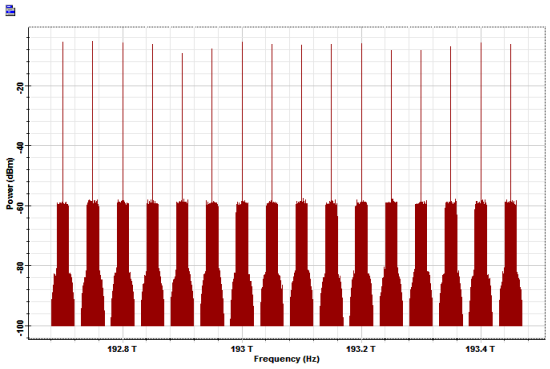

(a)

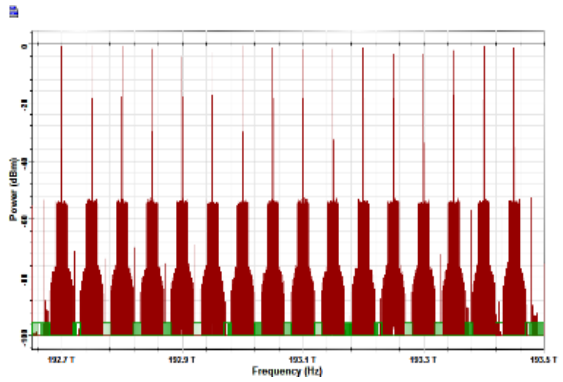

(b)

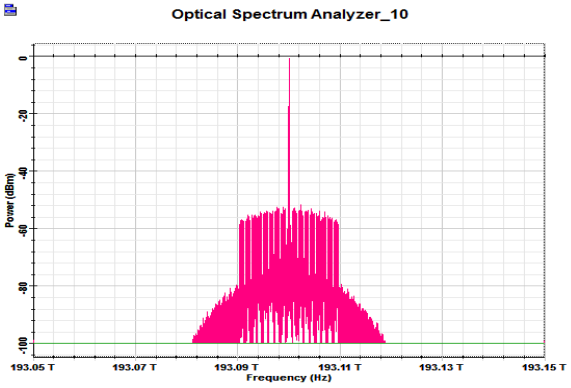

(c)

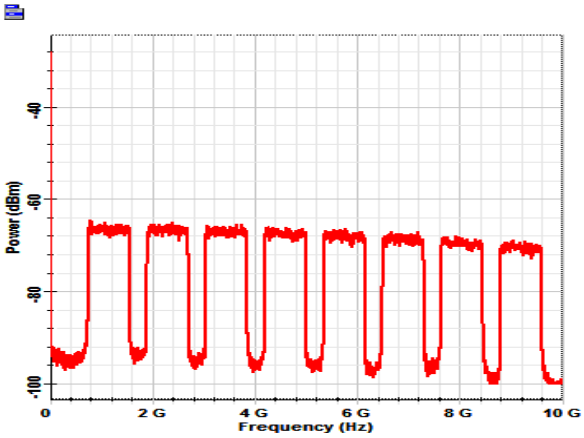

(d)

Figure 12. Results for 16-channel C-band WDM mobile fronthaul designed with 5 km-SMF. Each optical channel has P_T = 0 dBm and modulated by 8x1 GHz-bandwidth mobile signals having 64QAM modulation format (a) WDM signal at the fiber input. (b) WDM signal at the fiber output. (c) Ninth demultiplexed optical channel. (d) Spectrum of the detected ninth optical channel

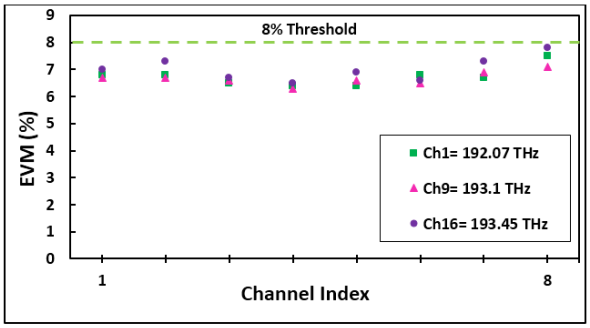

Figure 13. Variation of EVM with IF carrier index for 1st, 9th, and 16th optical channels in 16-channel C-band WDM mobile fronthaul. Eight IF carriers for each optical channel, P_T = 0 dBm, 64QAM format, and L= 5 km

REFERENCES

[1] N. U. Hasan, W. Ejaz, N. Ejaz, H. S. Kim, A. Anpalagan, and M. Jo, "Network selection and channel allocation for spectrum sharing in 5G heterogeneous networks", IEEE Access, vol. 4, pp. 980-992, 2016.

[2] C. Ranaweera, E. Wong, A. Nirmalathas, C. Jayasundara, and C. Lim, "5G C-RAN With Optical Fronthaul: An Analysis From a Deployment Perspective", IEEE Journal of Lightwave Technology, vol. 36, no. 11, pp. 2059-2068, 2018.

[3] M. Fiorani, A. Rostami, L. Wosinska, and P. Monti, "Abstraction models for optical 5G transport networks", Journal of Optical Communications and Networking, vol. 8, no. 9, pp. 656-665, September 2016.

[4] I. F. Akyildiz, S. C. Lin, and P. Wang, "Wireless software-defined networks (W-SDNs) and network function virtualization (NFV) for 5G cellular systems: An overview and qualitative evaluation," Computer Networks, vol. 93, no. 1, p. 66–79, December 2015.

[5] S. Zhang, Q. Wu, S. Xu, and G. Y. Li, "Fundamental green tradeoffs: progresses, challenges, and impacts on 5G networks," IEEE Communications Surveys and Tutorials, vol. 19, pp. 33-56, 2017.

[6] M. Ataee and A. Mohammadi, "Energy-efficient resource allocation for adaptive modulated MIMO–OFDM heterogeneous cloud radio access networks", Wireless Personal Communications, vol. 95, no. 4, pp. 4847-4866, Augest 2017.

[7] S. Iezekiel, "Radio-over-fiber technology and devices for 5G: an overview", Broadband Access Communication Technologies, vol. 9772, 2016.

[8] C. I. Badoi, N. Prasad and R. Prasad, "Virtualization and scheduling methods for 5G cognitive radio based wireless networks," Wireless Personal Communications, vol. 89, no. 2, pp. 599–619, July 2016.

[9] A. N. Rashed and M. S. Tabbour, "Suitable optical fiber communication channel for optical nonlinearity signal processing in high optical data rate systems", Wireless Personal Communications, vol. 97, no. 1, pp. 397–416, November 2017.

[10] S. Guo, S. Shao, Y. Wang, and H. Yang, "Cross stratum resources protection in fog-computing-based radio over fiber networks for 5G services", Optical Fiber Technology, vol. 37, pp. 61-68, September 2017.

[11] G. Kalfas, J. Vardakas, L. Alonso, C. Verikoukis, and N. Pleros, "Non-saturation delay analysis of medium transparent MAC protocol for 5G 60 GHz fiber-wireless towards 5G mmWave networks", Journal of Lightwave Technology, vol. 85, no. 18, pp. 3945-3955, September 2017.

[12] S. A. Haider, M. J. Zhao, and I. Ngebani, "MIMO beamforming architecture in millimeter wave communication systems", Wireless Personal Communications, vol. 97, no.2, pp. 2597–2616, November 2017.

[13] A. Ichkov, V. Atanasovski, and L. Gavrilovska, "Potentials for application of millimeter wave communications in cellular networks", Wireless Personal Communications, vol. 92, no. 1, pp. 279–295, January 2017.

[14] Y. Niu, Y. Li, D. Jin, Su, and A. V. Vasilakos, "A survey of millimeter wave communications (mmWave) for 5G: opportunities and challenges", Wireless Networks, vol. 21, no. 8, pp. 2657-2676, November 2015.

[15] M. Xiao, S. Mumtaz, Y. Huang, L. Dai, Y. Li, M. Matthaiou, G. K. Karagiannidis, E. Bjornson, K. Yang, I. C. Lin, and A. Ghosh, "Millimeter wave communications for future mobile networks, part I", IEEE Journal on Selected Areas in Communications, vol. 35, no. 7, pp. 1425-1431, July 2017.

[16] P. T. Dat, A. Kanno, N. Yamamoto, and T. Kawanishi, "5G transport and broadband access networks: the need for new technologies and standards", ITU Kaleidoscope: Trust in the Information Societ, Barcelona, Spain, 2015.

[17] J. Deng, O. Tirkkonen, R. F. Hollanti, T. Chen, and N. Nikaein, "Resource allocation and interference management for opportunistic relaying in integrated mmWave/sub-6 GHz 5G networks", IEEE Communications Magazine, vol. 55, no. 6, pp. 94-101, June 2017.

[18] A. Alnoman and A. Anpalagan, "Towards the fulfillment of 5G network requirements: technologies and challenges", Telecommunication Systems, vol. 65, no. 1, pp. 101–116, May 2017.

[19] K. Sakaguchi, E. M. Mohamed, H. Kusano, and S. Namba, "Millimeter-wave wireless LAN and its extension toward 5G heterogeneous networks", IEICE Transactions on Communications, vol. E98-B, no. 10, pp. 1932-1947 October 2015.

[20] M. Tesanovic and M. Nekovee, "mmWave-based mobile access for 5G: key challenges and projected standards and regulatory roadmap", Global Communications Conference (GLOBECOM), California, USA, 2015.

[21] J. Beas, G. Castañón, F. Orozco, I. Aldaya, A. A. Zavala, and G. Campuzano, "Knowledge-based framework for the design of millimeter-wave (60 GHz) radio over fiber land networks", Photonic Network Communications, vol. 30, no. 2, pp. 234-260, October 2015.

[22] F. C. Abrecht, R. Bonjour, S. Welschen, A. Josten, B. Baeuerle, D. Hillerkuss, M. Burla, and J. Leuthold, "Pre-equalization technique enabling 70 Gbit/s photonic-wireless link at 60 GHz", Optics Express, vol. 24, no. 26, pp. 30350-30359, 2016.

[23] J. Isabona and V. M. Srivastava, "Downlink massive MIMO systems: achievable sum rates and energy efficiency perspective for future 5G systems", Wireless Personal Communications, vol. 96, no. 2, pp. 2779-2796, September 2017.

[24] G. Liu, X. Hou, F. Wang, J. Jin, H. Tong, and Y. Huang, "Achieving 3D-MIMO with massive antennas from theory to practice with evaluation and field trial results", IEEE Systems Journal, vol. 11, no. 1, pp. 62-71, March 2017.

[25] L. Wang, H. Q. Ngo, M. Elkashlan, T. Q. Duong, and K. K. Wong, "Massive MIMO in spectrum sharing networks: achievable rate and power efficiency", IEEE Systems Journal, vol. 11, no. 1, pp. 20-31, March 2017.

[26] R. Mahapatra, "Participation of optical backbone network in successful advancement of wireless network," Wireless Personal Communications, vol. 96, no. 3, pp. 3463-3481, October 2017.

[27] O. Hayat, R. Ngah, and Y. Zahedi, "Cooperative device-to-device discovery model for multiuser and OFDMA network base neighbour discovery in in-band 5G cellular networks," Wireless Personal Communications, pp. 1-15, August 2017.

[28] K. Habel, M. Koepp, S. Weide, L. Fernandez, C. Kottke, and V. Jungnickel, "100G OFDM-PON for converged 5G networks: from concept to real-time prototype", Optical Fiber Communications Conference (OFC), California, USA, 2017.

[29] V. D. Esposti, F. Fuschini, R. S. Thomae, R. Mueller, D. Dupleich, K. Haneda, J. M. M. G. Pardo, J. P. Garcia, D. P. Gaillot, S. Hur, and M. Nekovee, "Millimeter-wave propagation: characterization and modeling toward fifth-generation systems", IEEE Antennas and Propagation Magazine, vol. 58, no. 6, pp. 115-127, December 2016.

[30] K. Sakaguchi, G. K. Tran, H. Shimodaira, S. Nanba, T. Sakurai, K. Takinami, I. Sidud, E. C. Strinati, A. Capone, I. Karls, R. Arefi, and T. Hauste, "Millimeter-wave evolution

for 5G cellular networks", IEICE Transactions on Communication, vol. E98-B, no. 3, pp. 388-402, March 2015.

[31] T. Yang, M. Gao, J. Qian, J. Zhang, and W. Chen "A flexible millimeter-wave radio-over-fiber system for various transmission bit rate", Optics and Laser Technology, vol. 96, pp. 132-140, November 2017.

[32] X. Yu, M. Matsuura, and Y. Yamao, "Composite effect of E/O nonlinearity and optical echo on EPWM-OFDM transmission in radio over fiber channel", Wireless Personal Communications, vol. 93, no. 3, pp. 647–660, April 2017.

[33] M. Kong and W. Zhou, "Delivery of 12QAM single carrier signal in a MIMO radio-over-fiber system at 60 GHz", IEEE Photonics Journal, vol. 9, no. 3, June 2017.

[34] Y. Yu, C. Ranaweera, C. Lim, L. Guo, Y. Liu, A. Nirmalathas, and E. Wong, "Hybrid fiber-wireless network: an optimization framework for survivable deployment", IEEE Journal of Optical Communications and Networking, vol. 9, no. 6, pp. 466-478, June 2017.

[35] S. Mikroulis, O. Omomukuyo, M. P. Thakur, and J. E. Mitchell, "Investigation of a SMF-MMF link for a remote heterodyne 60-GHz OFDM RoF based gigabit wireless access topology", IEEE Journal of Lightwave Technology, vol. 32, no. 20, pp. 3645-3653, October 2014.

[36] M. Fiorani, S. Tombaz, J. Martensson, B. Skubic, L. Wosinska, and P. Monti, "Modeling energy performance of C-RAN with optical transport in 5G network scenarios", IEEE Journal of Optical Communications and Networking, vol. 8, no. 11, pp. B21-B34, November 2016.

[37] F. Musumeci, C. Bellanzon, N. Carapellese, M. Tornatore, A. Pattavina, and S. Gosselin, "Optimal BBU placement for 5G C-RAN deployment over WDM aggregation networks", IEEE Journal of Lightwave Technology, vol. 34, no. 8, pp. 1963-1970, April 2016.

[38] W. HY, C. YC, and L. GR, "Remote beating of parallel or orthogonally polarized dual-wavelength optical carriers for 5G millimeter-wave radio-over-fiber link", Optic Express, vol. 42, no. 16, pp. 17654-17669, August 2016.

[39] C. Y. Lin, Y. C. Chi, C. T. Tsai, H. Y. Wang, H. Y. Chen, M. Xu, G. K. Chang, and G. R. Lin, "Millimeter-wave carrier embedded dual-color laser diode for 5G MMW of Link", IEEE Journal of Lightwave Technology, vol. 35, no. 12, pp. 2409-2420, June 2017.

[40] C. Lin, Y. C. Chi, C. T. Tsai, H. Y. Chen, and J. R. Lin, "Two-color laser diode for 54-Gb/s fiber-wired and 16-Gb/s MMW wireless OFDM transmissions", Photonics Research, vol. 5, no. 4, pp. 271-279, August 2017.

[41] D. Boviz, C. S. Chen, and S. Yang, "Effective design of multi-user reception and fronthaul rate allocation in 5G cloud RAN", IEEE Journal on Selected Areas in Communications, vol. 35, no. 8, pp. 1825-1836, August 2017.

[42] H. Zhang, Y. Dong, J. Cheng, Md. J. Hossain, and V. C. M. Leung, "Fronthauling for 5G LTE-U ultra dense cloud small cell networks ", IEEE Wireless Communications , vol. 23, no. 6, pp. 48-53, December 2016.

[43] M. Sung, S-H Cho, H. S. Chung, S. M. Kim, and J. H. Lee, "Investigation of transmission performance in multi-IFoF based mobile fronthaul with dispersion-induced intermixing noise mitigation," Optic Express, vol. 25, no. 8, pp. 9346-9357, April 2017.

[44] M. Xu, F. Lu, J. Wang, L. Cheng, D. Guidotti, and G-K Chang, "Key technologies for next-generation digital RoF mobile fronthaul with statistical data compression and multiband modulation", IEEE Journal of Lightwave Technology, vol. 35, no. 17, pp. 3671-3679, September 2017.

[45] T. Pfeiffer, "Next generation mobile fronthaul and midhaul architectures", Journal of Optical Communications and Networking, vol. 7, no. 11, pp. B38-B45, November 2015.

[46] X. Liu, H. Zeng, N. Chand, and F. Effenberger, "Efficient mobile fronthaul via DSP-based channel aggregation", IEEE Journal of Lightwave Technology, vol. 34, no. 6, pp. 1556-1564, March 2016.

[47] D. Chitimalla, K. Kondepu, L. Valcarenghi, M. Tornatore, and B. Mukherjee, "5G fronthaul-latency and jitter studies of CPRI over ethernet", IEEE Journal of Optical Communications and Networking, vol.9, no. 2, pp. 172-182, February 2017.

[48] L. Valcarenghi, K. Kondepu, and P. Castoldi, "Time- versus size-based CPRI in ethernet encapsulation for next generation reconfigurable fronthaul", IEEE Journal of Optical Communications and Networking, vol. 9, no. 9, pp. D64-D73, 2017.

[49] H. Zeng, X. Liu, S. Megeed, N. Chand, and F. Effenberger, "Real-time demonstration of CPRI-compatible efficient mobile fronthaul using FPGA", IEEE Journal of Lightwave Technology, vol. 35, no. 6, pp. 1241-1247, March 2017.

[50] X. Liu, H. Zeng, N. Chand, and F. Effenberger, "Efficient mobile fronthaul via DSP-based channel aggregation", IEEE Journal of Lightwave Technology, vol. 34, no. 6, pp. 1556-1564, March 2016.

[51] M. Sung, S-H Cho, H. S. Chung, S. M. Kim, and J. H. Lee, "Investigation of transmission performance in multi-IFoF based mobile fronthaul with dispersion-induced intermixing noise mitigation" Optic Express, vol. 25, no. 8, pp. 9346-9357, April 2017.

[52] F. Lu, M. Xu, L. Cheng, J. Wang, S. Shen, J. Zhang, and G-K Chang, "Sub-band pre-distortion for PAPR reduction spectral efficient 5G mobile fronthaul", IEEE Photonic Technology Letters, vol. 29, no. 1, pp. 122-125, January 2017.

[53] Y. Tian, K-L Lee, C. Lim, and A. Nirmalathas, "60 GHz analog radio-over-fiber fronthaul investigations", IEEE Journal of Lightwave Technology, vol. 35, no.19, pp. 4304-4310, October 2017.

[54] P. Aggarwal and V. A. Bohara, "On the multiband carrier aggregated nonlinear LTE-A system", IEEE Access, vol. 5, pp. 16930-16943, 2017.

[55] S. Lange, S. Wolf, J. Lutz, L. Altenhain, R. Schmid, R. Kaiser, C. Koos, S. Randel, and M. Schell, "100 GBd intensity modulation and direct detection with an InP-based monolithic DFB laser Mach-Zehnder modulator", Optical Fiber Communications Conference and Exhibition (OFC), California, USA, 2017.

[56] N. H. Zhu, Z. Shi, Z. K. Zhang, Y. M. Zhang, C. W. Zou, Z. P. Zhao, Y. Liu, W. Li, and M. Li, "Directly modulated semiconductor lasers", IEEE Journal of Selected Topics in

Quantum Electronics, vol. 24, no. 1, February 2018.

[57] G. N. Liu, L. Zhang, T. Zuo, Q. Zhang, J. Zhou, and E. Zhou, "IM/DD transmission techniques for emerging 5G fronthaul, DCI and metro applications", Optical Fiber Communications Conference and Exhibition (OFC), California, USA, 2017.

[58] T. Shao, E. P. Martin, P. M. Anandarajah, and L. P. Barry, "60-GHz direct modulation-direct detection OFDM-RoF system using gain-switched laser", IEEE Photonics Technology Letters, vol. 27, no. 2, pp. 193-196, January 2015.

[59] S. A. Khwandah, J. P. Cosmas, I. A. Glover, P. I. Lazaridis, N. R. Prasad, and Z. D. Zaharis, "Direct and external intensity modulation in OFDM RoF links", IEEE Photonics Journal, vol. 7, no. 4, August 2015.

[60] X. Liu, F. Effenberger, N. Chand, L. Zhou, and H. Lin, "Efficient mobile fronthaul transmission of multiple LTE-A signals with 36.86-Gb/s CPRI-equivalent data rate using a directly-modulated laser and fiber dispersion mitigation", Asia Communications and Photonics Conference, Shanghai China, 2014.

[61] X. Liu, H. Zeng, N. Chand, and F. Effenberger, "Experimental demonstration of high-throughput low-latency mobile fronthaul supporting 48 20-MHz LTE signals with 59-Gb/s CPRI-equivalent rate and 2-μs processing latency," European Conference Optical Communication, Valencia, Spain, 2015.

[62] M. Sung, S-H Cho, K. S. Kim, H-K Kwon, B-S Kang, D S Oh, D-S Lyu, H. Lee, S. M. Kim, J. H. Lee, and H. S. Chung, "Demonstration of IFoF based 5G mobile fronthaul in 28 GHz millimeter wave testbed supporting giga-bit mobile services", Optical Fiber Communications Conference and Exhibition (OFC), California, USA, 2017.

[63] Zh. Yu, Y. Lou, M. Chen, H. Chen, S. Yang, and S. Xie, "Adaptive three-dimensional optimization for optical direct-detection OFDM", IEEE Journal of Lightwave Technology, vol. 35, no. 9, pp. 506-1512, May 2017.

[64] J. Zhang, Y. Zheng, X. Hong, and C. Guo, "Increase in capacity of an IM/DD OFDM-PON using super-nyquist image-induced aliasing and simplified nonlinear equalization", IEEE Journal of Lightwave Technology, vol. 35, no. 16, pp. 4105-4113, October 2017.

[65] J. Shi, Y. Zhou, Y. Xu, J. Zhang, J. Yu, and N. Chi, "200-Gbps DFT-S OFDM using DD-MZM-based twin-SSB with a MIMO-volterra equalizer", IEEE Photonics Technology Letters, vol. 29, no. 14, pp. 1183-1186, July 2017.

[66] J-W Wu, Q. Qiu, X-P Zhang, and Y. H. Won, "Simultaneous generation of microwave, millimeter-wave, and terahertz photonic signal based on two-color semiconductor laser subject to single-beam optical injection", IEEE Journal of Selected Topics in Quantum Electronics, vol. 23, no. 4, August 2017.

[67] O. Strobel, "Optical and microwave technologies for telecommunication networks", John Wiley & Sons, Ltd, United Kingdom, 2016.

[68] H-Y Chen, Y-C Chi, C-Y Lin, and G-R Lin, "Adjacent channel beating with recombined dual-mode colorless FPLD for MMW-PON", IEEE Journal of Selected Topics in Quantum Electronics, vol. 23, no. 6, December 2017.

[69] X. Liu, F. Effenberger, N. Chand, L. Zhou, and H. Lin, "Demonstration of bandwidth-efficient mobile fronthaul enabling seamless aggregation of 36 E-UTRA-like wireless signals in a single 1.1-GHz wavelength channel", Optical Fiber Communication Conference, paper M2J.2, 2015.

[70] M. Hudlicka, C. Lundstrom, D. A. Humphreys, and I. Fatadin, "BER estimation from EVM for QPSK and 16-QAM coherent optical systems", IEEE, 6th International Conference on Photonics (ICP), Kuching, Malaysia, 2016.

[71] G. H. Smith, D. Novak, and Z. Ahmed, "Overcoming chromatic-dispersion effects in fiber-wireless systems incorporating external modulators", IEEE Transactions on Microwave Theory and Techniques, vol. 45, no. 8, pp. 1410-1415, Aug. 1997.